Available online at www.sciencedirect.com

ScienceDirect

Procedia Structural Integrity 42 (2022) 614–622

Structural Integrity Procedia

www.elsevier.com/locate/procedia

23rd European Conference on Fracture – ECF23

Failure analysis of a composite riser pipe under operational and spooling loads

James C. Hastie[a], Igor A. Guz[b,*], Maria Kashtalyan[a]

[a] *Centre for Micro- and Nanomechanics (CEMINACS), School of Engineering, University of Aberdeen, AB24 3FX, Scotland, U.K*
[b] *School of Engineering and Physical Sciences, Heriot-Watt University, Edinburgh EH14 4AS, Scotland, U.K.*

Abstract

Fibre-reinforced plastic riser pipes are on the cusp of deployment in deep waters where high specific strengths and moduli and corrosion resistance are highly advantageous. In this work, failure analysis is performed for thermoplastic composite pipe (TCP) under loads illustrative of deepwater riser operation by finite element modelling. Temperature-dependent material properties are considered. Different laminate stacking sequences are analysed and a multi-angle stack is shown to be effective for both small and large tension operating scenarios. The bending of TCP at reduced and elevated temperatures, representative of spooling in different environments, is also investigated. Temperature change causes deviation from the symmetry expected between stresses at tensile (top) and compressive (bottom) sides of the pipe under simple bending. It is shown that TCP can be optimised for spooling by orientating unidirectional layers at an 'intermediate' angle that promotes utilisation of in-plane shear strength, rather than fibre or transverse strengths. Since optimising the stacking sequence for operation and spooling are effectively mutually exclusive, large spools will inevitably be required for TCP designed to operate in extreme in-service conditions.

Keywords: Finite element modelling; thermomechanical analysis; composite failure criteria

1. Introduction

Lightweight thermoplastic composite pipe (TCP), consisting of fibre-reinforced thermoplastic laminate with unreinforced thermoplastic inner and outer liners (Fig. 1), is ideal for riser applications in deep waters where the weight of traditional metallic counterparts is a limiting factor. During operation the pipe is subjected to pressure and tension in combination with large through-wall thermal gradients that arise from the mismatch between temperatures

* Corresponding author.
E-mail address: i.guz@hw.ac.uk

10.1016/j.prostr.2022.12.078

of the pipe contents and surrounding ocean. When spooled onto a storage drum, the pipe is subjected to large bending moments potentially in different thermal environments as TCP is deployed worldwide.

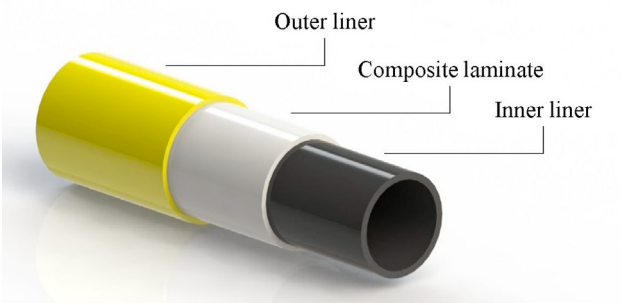

Fig. 1. TCP layers

The behaviour of fibre-reinforced plastic (FRP) pipes has been studied for many years. Numerous studies have considered the application of mechanical loads in isolation (Guz et al. 2017; Menshykova and Guz 2014) and in combinations (Meniconi et al. 2001; Amaechi et al. 2019; Cox et al. 2019) relevant to offshore scenarios. Thermomechanical response has been less widely investigated. Experimental work has included pressure (Onder et al. 2009; Sayman et al. 2011) or tensile (Ortenzi et al. 2012) tests performed at different temperatures, which have generally revealed strength reductions at high temperatures and strong dependence on fibre angle. The bulk of modelling work has involved analytical formulations for uniform temperature change, e.g. pertaining to post-manufacturing cool-down or operational heating, applied in isolation (Yuan 1993) or combined with pressure (Xia et al. 2001) or axial loads (Tzeng and Chien 1994). Thermal gradient problems have been analysed (Çallıoğlu et al. 2008; Bakaiyan et al. 2009). Finite element (FE) modelling would allow a variety of loads to be introduced once a base model is established. Furthermore, defects can be introduced and studied whereas this may prove complex or unfeasible analytically. It is notable that the temperature dependency of material properties has often been overlooked in preceding thermomechanical studies, particularly for thick-walled analyses due most likely to the unavailability of data needed to fully define the unidirectional materials and costs/practical limitations associated with extensive experimental programs.

In a previous work by the authors, an FE model was developed for stress analysis of TCP subjected to combined pressures, axial tension and through-wall thermal gradient illustrative of a single-leg hybrid riser system (Hastie et al. 2019a). Material temperature dependency was accounted for. Maximum Stress and Tsai-Hill failure indices for laminate layers were examined for different operating load cases and further scenarios were investigated in Hastie et al. (2019b). Hashin failure analysis was performed in Hastie et al. (2020). Material failure coefficients for TCP under combined bending and uniform thermal load representative of spooling in different environments have also been examined (Hastie et al. 2021a,b). In the present work, strength ratios are evaluated for the TCP layers in operation and when spooled and the implications of optimising the stacking sequence for either stage are discussed.

2. Methodology

2.1. Finite element models

Three-dimensional (3D) FE models were developed in Abaqus/CAE and validated against 3D elasticity solutions, as outlined in Hastie et al. (2019a, 2021b). The operating load model is shown in Fig. 2. Internal and external pressures (P_i, P_e) are applied directly on the pipe surfaces. Tension force (F_z) is applied on a reference point located at the centre of one end. All pipe end degrees of freedom except the radial translation are constrained to the point using a kinematic coupling. A reference point and coupling is used to fix the opposite end. Thermal loads are applied simultaneously in the same analysis step. Internal surface temperature (T_i) is applied as a boundary condition

and on the external surface a film condition simulates free convection based on surrounding temperature, T_∞, and heat transfer coefficient, h_c. An initial temperature is applied as a predefined field to the entire part prior to the coupled temperature-displacement step.

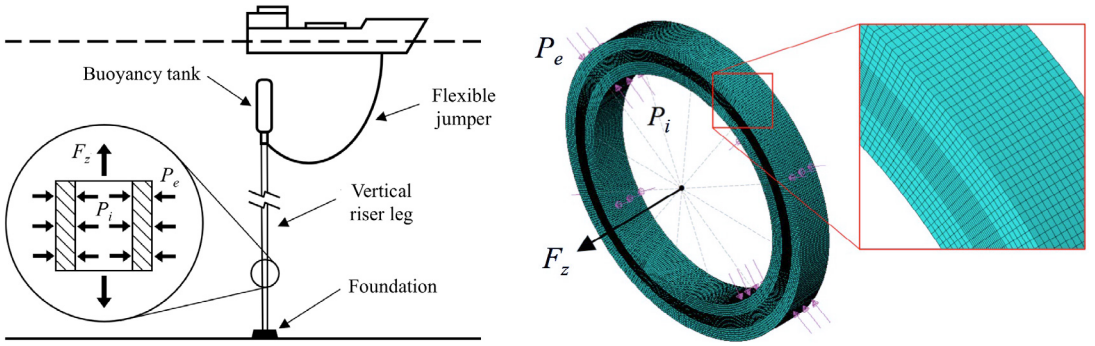

Fig. 2. Operating load model

The spooling model is shown in Fig. 3. Bending is imposed via rotations applied to reference points at each end of the pipe, rigidly coupled to the pipe end faces. The total angle of rotation is L/R, where L is the length of the pipe and R is the bending radius ($R = 1/K$; K is the curvature). Uniform temperature, T, is applied simultaneously with bending in a coupled-temperature displacement step. Initial temperature is defined using a predefined field.

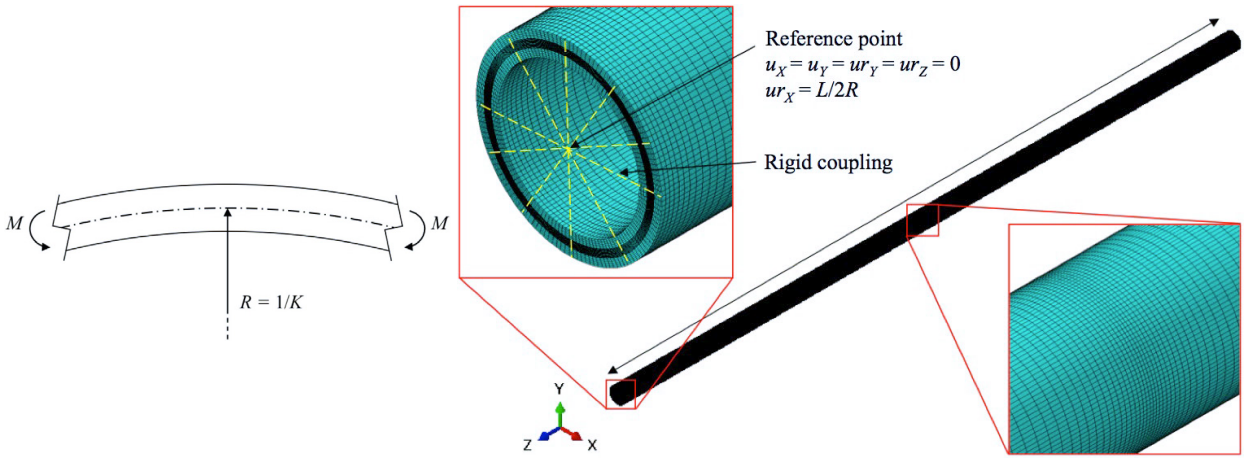

Fig. 3. Spooling model (model end conditions symmetric at opposite end)

2.2. Pipe configuration and materials

The pipe dimensions resemble real-world products without emulating any one in particular. Internal and external radii are 76 mm and 100 mm respectively. The inner liner, FRP laminate and outer liner are each 8 mm thick. The laminate comprises eight 1 mm-thick unidirectional layers. Four configurations, named A-D, with different laminate unidirectional layer orientations specified in Table 1 are studied.

The pipe comprises unidirectional AS4/APC-2 carbon/polyetheretherketone (PEEK) laminate layers and homogeneous PEEK inner and outer liner. Temperature-dependent material properties were previously compiled from literature and listed in Hastie et al. (2019a). Perfect layer bonding is assumed.

Table 1. Laminate stacking sequences

TCP	Stacking sequence
A	$[\pm 55]_4$
B	$[\pm 42.5]_4$
C	$[\pm 30]_4$
D	$[(\pm 55)_2/(\pm 30)_2]$

2.3. Failure criteria

Stresses computed using the FE models are used to evaluate failure of isotropic liners and FRP laminate. Liner yielding is evaluated according to the von Mises criterion. The von Mises stress is

$$\sigma_{vM} = \sqrt{\frac{(\sigma_1-\sigma_2)^2+(\sigma_2-\sigma_3)^2+(\sigma_3-\sigma_1)^2}{2}} \tag{1}$$

and the strength ratio is

$$S_r = \frac{\sigma_y}{\sigma_{vM}} \tag{2}$$

where σ_y is the yield strength. A ratio of $S_r \leq 1.0$ indicates failure.

In this study, first ply failure (FPF) of the laminate is evaluated according to Maximum Stress (herein "Max Stress") and Hashin criteria. The Max Stress theory assumes failure occurs when any lamina stress component exceeds the corresponding allowable. The failure index is

$$I_F = max\begin{Bmatrix} \sigma_1/X_T \;\; if \;\; \sigma_1 > 0 \;\; or \;\; |\sigma_1|/X_C \;\; if \;\; \sigma_1 < 0 \\ \sigma_2/Y_T \;\; if \;\; \sigma_2 > 0 \;\; or \;\; |\sigma_2|/Y_C \;\; if \;\; \sigma_2 < 0 \\ \sigma_3/Z_T \;\; if \;\; \sigma_3 > 0 \;\; or \;\; |\sigma_3|/Z_C \;\; if \;\; \sigma_3 < 0 \\ |\tau_{23}|/Q \\ |\tau_{13}|/R \\ |\tau_{12}|/S \end{Bmatrix} \tag{3}$$

where X, Y and Z are tensile and compressive strengths (subscripts 'T' and 'C') along material directions 1, 2 and 3 respectively; Q, R, S are shear strengths in planes 23, 13, 12 respectively. The strength ratio is the reciprocal:

$$S_r = \frac{1}{I_F} \tag{4}$$

Max Stress can be erroneous for off-axis loading where interaction amongst stresses within the layer become significant. In the criterion of Hashin (1980), fibre and matrix failures under tension and compression are distinguished and partial interaction of stresses accounted for. Sub-criteria for the separate modes are listed below.

Fibre in tension (when $\sigma_1 > 0$):

$$I_{Fft}^2 = max\left\{\left(\frac{\sigma_1}{X_T}\right)^2 + \frac{(\tau_{12}^2+\tau_{13}^2)}{R^2}, \left(\frac{\sigma_1}{X_T}\right)^2\right\} \tag{5a}$$

Fibre in compression ($\sigma_1 < 0$):

$$I_{Ffc}^2 = \left(\frac{\sigma_1}{X_C}\right)^2 \tag{5b}$$

Matrix in tension ($(\sigma_2 + \sigma_3) > 0$):

$$I_{Fmt}^2 = \frac{(\sigma_2 + \sigma_3)^2}{Y_T^2} + \frac{(\tau_{23}^2 - \sigma_2\sigma_3)}{Q^2} + \frac{(\tau_{12}^2 + \tau_{13}^2)}{R^2} \tag{5c}$$

Matrix in compression ($(\sigma_2 + \sigma_3) < 0$):

$$I_{Fmc}^2 = \left(\left(\frac{Y_C}{2Q}\right)^2 - 1\right)\frac{(\sigma_2 + \sigma_3)}{Y_C} + \frac{(\sigma_2 + \sigma_3)^2}{4Q^2} + \frac{(\tau_{23}^2 - \sigma_2\sigma_3)}{Q^2} + \frac{(\tau_{12}^2 + \tau_{13}^2)}{R^2} \tag{5d}$$

We note that the above are squares of the failure indices. The strength ratio based on Hashin is

$$S_r = \frac{1}{max\,(I_{Fft}, I_{Ffc}, I_{Fmt}, I_{Fmc})} \tag{6}$$

3. Results and discussion

3.1. Riser operation

We begin by examining the temperature distributions through the pipe wall for low and high internal operating temperatures. Distributions for T_i = 30 °C and 130 °C combined with T_∞ = 5 °C, h_c = 50 Wm^{-2}°C^{-1} on the outer surface are shown in Fig. 4 (distributions are the same for all configurations since they only differ in fibre angle rotated about the radial direction). Temperature at the outer surface exposed to free convection does not rise significantly with T_i. The drop in temperature is steeper through the liners (radius, r = 76 mm to 84 mm and 92 mm to 100 mm) than the composite laminate (r = 84 mm to 92 mm) as a result of lower through-liner thermal conductivity and thus greater insulating characteristics.

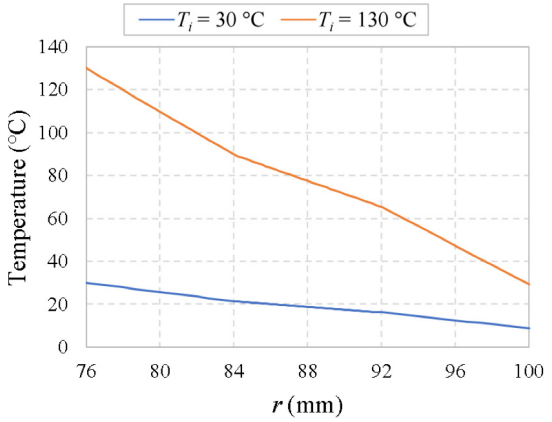

Fig. 4. Through-wall operating temperature distribution

The failure response of the configurations subjected to operating load combinations is now investigated. Layer strength ratios are summarised in Table 2 for the above temperature profiles combined with the following mechanical loads: P_i = 15 MPa, P_e = 10 MPa, F_z = 50 kN. The increase in internal temperature causes a substantial drop in strength ratio for the inner liner of all configurations. The laminate and outer liner are less affected, which follows less temperature change seen in Fig. 4. Given that the inner liner function is fluid containment, yielding does

not necessarily constitute a loss of function and therefore a low margin of safety may not be a limiting factor. Current guidelines dictate higher safety factors for brittle fibre-reinforced laminate layers (DNV GL, 2018). For the laminate the Hashin criterion is consistently more conservative (producing lower strength ratio) than Max Stress, owing to the inclusion of stress interaction effects that are absent from the Max Stress theory. The lowest laminate strength ratios are observed for TCP C with $[\pm 30]_4$ stacking sequence. TCP D with multi-angle laminate comprising both 55° and 30° layers is superior to TCPs A and B with angle-ply 55° and 42.5° stacking sequences respectively.

Table 2. Layer strength ratios: operation, F_z = 50 kN

T_i (°C)	TCP	Inner liner	Laminate		Outer liner
			Max Stress (mode)	Hashin (mode)	
30	A	12.82	12.50 (Out-of-plane comp.)	9.13 (Matrix comp.)	10.99
	B	12.82	12.50 (Out-of-plane comp.)	9.13 (Matrix comp.)	11.63
	C	10.20	11.91 (Transverse tens.)	7.67 (Matrix comp.)	10.10
	D	13.33	12.50[a] (Out-of-plane comp.)	9.54[a] (Matrix comp.)	11.77
130	A	1.25	8.77 (Out-of-plane comp.)	7.07 (Matrix comp.)	9.71
	B	1.25	8.93 (Out-of-plane comp.)	7.67 (Matrix comp.)	11.63
	C	1.47	6.37 (Transverse tens.)	5.20 (Matrix comp.)	7.46
	D	1.23	8.93[a] (Out-of-plane comp.)	8.17[a] (Matrix comp.)	12.20

[a]Value for 55° layer

Strength ratios for the same conditions with larger axial tension, F_z = 500 kN, are presented in Table 3. TCP C now exhibits the superior strength ratios for large axial tension and the higher angle counterparts, A and B, are comparatively less effective. TCP D comprising high and low angle layers also outperforms A and B and is effective for both F_z = 50 kN and 500 kN.

Table 3. Layer strength ratios: operation, F_z = 500 kN

T_i (°C)	TCP	Inner liner	Laminate		Outer liner
			Max Stress (mode)	Hashin (mode)	
30	A	4.26	2.85 (Transverse tens.)	2.81 (Matrix tens.)	4.17
	B	6.62	6.62 (Shear)	5.20 (Matrix comp.)	6.21
	C	10.20	12.35 (Out-of-plane comp.)	8.45 (Matrix comp.)	8.93
	D	8.00	7.75[a] (Transverse tens.)	6.20[a] (Matrix comp.)	7.30
130	A	1.23	2.41 (Transverse tens.)	2.26 (Matrix tens.)	3.29
	B	1.19	6.62 (Shear)	5.06 (Matrix comp.)	6.29
	C	1.48	9.09 (Out-of-plane comp.)	7.07 (Matrix comp.)	9.17
	D	1.30	7.09[b] (Fibre tens.)	6.09[a] (Matrix comp.)	7.75

[a]Value for 55° layer; [b]Value for 30° layer

3.2. Spooling

We now consider bending of the pipe at reduced and elevated temperatures representative of spooling in extreme thermal environments. Strength ratios for the configurations bent to R = 9 m at T = 0 °C and 50 °C are summarised in Table 4 and Table 5. Temperature change causes deviation from the symmetry of tensile/compressive stress magnitudes expected at top/bottom of the pipe according to simple bending theory. As a consequence, the liners exhibit lower strength ratio at the top of the pipe at 0 °C and at the bottom at 50 °C. Strength ratios for the TCP A laminate are noticeably lower at the top of the pipe where the lamina transverse stress is tensile and the relatively weak corresponding strength is utilised, compared to the bottom where the transverse component is compressive and

utilisation is lower. High fibre stresses are observed in layers orientated at 30° especially if these are combined with higher angle layers (TCP D), resulting in high utilisation of the compressive strength at the bottom of the pipe (since fibres are far stronger in tension than compression). The laminate can be optimised for spooling by orientating unidirectional layers at an 'intermediate' angle of 42.5° (TCP B) that promotes utilisation of the shear strength and avoids excessive stresses that develop along transverse or fibre directions.

Table 4. Layer strength ratios: spooling, R = 9m at T = 0 °C

TCP	Location	Inner liner	Laminate		Outer liner
			Max Stress (mode)	Hashin (mode)	
A	Top	2.80	1.43 (transverse tens.)	1.23 (matrix tens.)	2.37
	Bottom	3.03	2.19 (shear)	1.79 (matrix comp.)	2.57
B	Top	2.53	1.73 (shear)	1.62 (matrix tens.)	2.20
	Bottom	2.71	1.77 (shear)	1.74 (matrix comp.)	2.42
C	Top	2.24	1.70 (shear)	1.47 (fibre tens.)	2.02
	Bottom	2.42	1.64 (fibre comp.)	1.48 (matrix tens.)	2.23
D	Top	2.65	1.82[a] (transverse tens.)	1.41[a] (matrix tens.)	2.27
	Bottom	2.97	1.35[b] (fibre comp.)	1.35[b] (fibre comp.)	2.56

[a]Value for 55° layer; [b]Value for 30° layer

Table 5. Layer strength ratios: spooling, R = 9m at T = 50 °C

TCP	Location	Inner liner	Laminate		Outer liner
			Max Stress (mode)	Hashin (mode)	
A	Top	2.38	1.43 (transverse tens.)	1.19 (matrix tens.)	2.02
	Bottom	2.15	2.40 (shear)	1.84 (matrix comp.)	1.82
B	Top	2.13	1.78 (shear)	1.71 (matrix tens.)	1.91
	Bottom	1.96	1.74 (shear)	1.70 (matrix comp.)	1.70
C	Top	1.88	1.85 (shear)	1.55 (fibre tens.)	1.75
	Bottom	1.73	1.69 (shear)	1.34 (matrix tens.)	1.56
D	Top	2.34	2.04[a] (transverse tens.)	1.55[a] (matrix tens.)	2.02
	Bottom	2.04	1.38[b] (fibre comp.)	1.38[b] (fibre comp.)	1.74

[a]Value for 55° layer; [b]Value for 30° layer

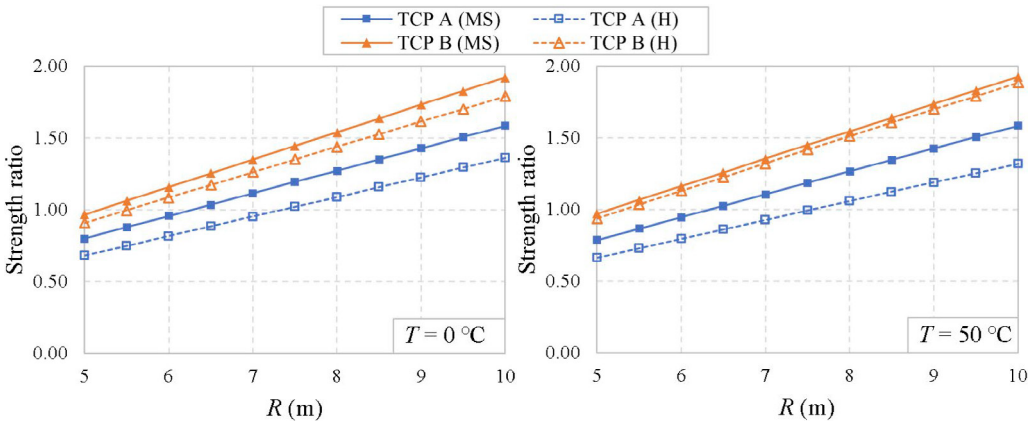

Fig. 5. Minimum laminate Max Stress (MS) and Hashin (H) strength ratios vs. bending radius at temperature

The minimum laminate strength ratios (of top and bottom) for TCPs A and B over the range R = 5 m to 10 m at 0 °C and 50 °C are shown in Fig. 5 to demonstrate how fibre angle influences practical minimum bending radius. Failure of the TCP A laminate occurs at approximately R = 7.5 m at both temperatures according to the Hashin criterion. Meanwhile, failure of the TCP B laminate occurs when R = 5.5 m at 0 °C and approximately 5.25 m at 50 °C. Hashin strength ratios of 1.35 and 1.42 are observed for TCP B when bent to R = 7.5 m, in other words the failure radius of TCP A, at 0 °C and 50 °C respectively.

3.3. Discussion

A multi-angle stack with high and low fibre angle layers is shown to be effective for both small and large tension operating scenarios. Meanwhile, the laminate can be optimised for spooling by orientating the unidirectional layers at an intermediate fibre angle that avoids excessive fibre or transverse stresses. Alas, optimising the laminate for operating conditions and spooling are in effect mutually exclusive. It therefore appears unavoidable that large radius spools, which have a direct bearing on installation vessel sizes and ancillary equipment, will be required for the storage and transportation of TCP designed to operate under the most extreme in-service conditions. This compounds the fact that the spools must have sufficient size capacity to store the very long pipe lengths intended for deep waters but is not necessarily disconcerting given that installation of TCP is characteristically more economical than that of heavier metallic pipes. Nevertheless, requirements for vessel and accompanying equipment must be factored into offshore deployment plans.

4. Conclusions

In this work, stresses in TCP subjected to combined mechanical and thermal loads were analysed by FE modelling. Yielding of plastic liners and failure of FRP layers according to Max Stress and Hashin criteria were evaluated for operating and spooling load cases. Optimising the laminate stacking sequence for operation will adversely affect spooling capacity and vice-versa. Thus, TCP intended for extreme operating conditions will invariably require large diameter storage spools with implications for installation vessel sizes, lifting equipment and so on. Future work should be directed at scrutinising the physical accuracy of lamina failure criteria for the combined load cases. This can be undertaken with a view to reducing the safety factors required in current design guidelines.

References

Amaechi, C.V., Gillett, N., Odijie, A.C., Hou, X., Ye, J., 2019. Composite risers for deep waters using a numerical modelling approach. Composite Structures 210, 486-499.

Bakaiyan, H., Hosseini, H., Ameri, E., 2009. Analysis of multi-layered filament-wound composite pipes under combined internal pressure and thermomechanical loading with thermal variations. Composite Structures 88(4), 532-541.

Çallıoğlu, H., Ergun, E., Demirdağ, O., 2008. Stress analysis of filament-wound composite cylinders under combined internal pressure and thermal loading. Advanced Composites Letters 17(1), 13-21.

Cox, K., Menshykova, M., Menshykov, O., Guz, I., 2019. Analysis of flexible composites for coiled tubing applications. Composite Structures 225, 111118.

DNV GL, 2018. Standard DNVGL-ST-F119 Thermoplastic composite pipes.

Guz, I.A., Menshykova, M., Paik, J.K., 2017. Thick-walled composite tubes for offshore applications: an example of stress and failure analysis for filament-wound multi-layered pipes. Ships and Offshore Structures 12(3), 304-322.

Hashin, Z., 1980. Failure criteria for unidirectional fiber composites. Journal of Applied Mechanics 47(2), 329-334.

Hastie, J.C., Guz, I.A., Kashtalyan, M., 2019a. Effects of thermal gradient on failure of a thermoplastic composite pipe (TCP) riser leg. International Journal of Pressure Vessels and Piping 172, 90-99.

Hastie, J.C., Kashtalyan, M., Guz, I.A., 2019b. Failure analysis of thermoplastic composite pipe (TCP) under combined pressure, tension and thermal gradient for an offshore riser application. International Journal of Pressure Vessels and Piping 178, 103998.

Hastie, J.C., Guz, I.A., Kashtalyan, M., 2020. Structural integrity of deepwater composite pipes under combined thermal and mechanical loading. Procedia Structural Integrity 28, 850-863.

Hastie, J.C., Kashtalyan, M., Guz, I.A., 2021a. Analysis of filament-wound sandwich pipe under combined internal pressure and thermal load considering restrained and closed ends. International Journal of Pressure Vessels and Piping 191, 104350.

Hastie, J.C., Guz, I.A., Kashtalyan, M, 2021b. Numerical modelling of spoolable thermoplastic composite pipe (TCP) under combined bending and thermal load. Ships and Offshore Structures, DOI: 10.1080/17445302.2021.1958534.

Meniconi, L.C.M., Reid, S.R., Soden, P.D., 2001. Preliminary design of composite riser stress joints. Composites Part A: Applied Science and Manufacturing 32(5), 597-605.

Menshykova, M., Guz, I.A., 2014. Stress analysis of layered thick-walled composite pipes subjected to bending loading. International Journal of Mechanical Sciences 88, 289-299.

Onder, A., Sayman, O., Dogan, T., Tarakcioglu, N., 2009. Burst failure load of composite pressure vessels. Composite Structures 89(1), 159-166.

Ortenzi, A., de Carvalho, J., Corvi, A., 2012. Comparison behavior of tensile tests for GFRP filament wound pipes with two different sectional areas regarding high temperature, 31st International Conference on Ocean, Offshore and Arctic Engineering. Rio de Janeiro, Brazil, 1–6 July. ASME, 955-961.

Sayman, O., Deniz, M.E., Dogan, T., Yaylagan, E., 2011. Failure pressures of composite cylinders with a plastic liner. Journal of Reinforced Plastics and Composites 30(10), 882-888.

Tzeng, J.T., Chien, L.S., 1994. A thermal/mechanical model of axially loaded thick-walled composite cylinders. Composites Engineering 4(2), 219-232.

Xia, M., Kemmochi, K., Takayanagi, H., 2001. Analysis of filament-wound fiber-reinforced sandwich pipe under combined internal pressure and thermomechanical loading. Composite Structures 51(3), 273-283.

Yuan, F.G., 1993. Thermal stresses in thick laminated composite shells. Composite Structures 26(1–2), 63-75.